

Non-Hermitian curved space via inverted wave equation

C. Zhang (张春娟)¹, Y. Liu (刘泱杰)^{1,*} H. Lin², and Bin Zhou^{1, 3}

¹ Department of Physics, School of Physics, Hubei University, Wuhan 430062, Hubei Province

² College of Physical Science and Technology, Central China Normal University, Wuhan 430079, Hubei Province

³ Wuhan Institute of Quantum Technology, Wuhan 430206, Hubei Province

(Dated: 11st Feb. '26, manuscript ID #591962 for *Opt. Lett.*)

Inverting design method of solving passive graded materials from predefined amplitude and phase was developed along the line of transformation optics (TO), which however precludes the presence of source and sink in the pragmatic world. So in this Letter we extend such an inverse method to non-Hermitian media, offering more freedom to manipulate the wave flows. Our principle of a curved-space analogue picture powered with gain and loss, is exemplified by three types: amplitude controlling, phase conversion, and direction shunting. Our numeric examples showcase precise wave manipulation in a surprisingly simple manner, which goes beyond convectional paradigms of TO and is readily implementable in realistic photonic platform.

I. INTRODUCTION

To control waves in both amplitude and phase from first principle, one inversely designs inhomogeneous metamaterials accessible to state-of-the-art, which saves the heavy computation price forwardly performed. So we directly solve material profiles by predefining waves, and this methodology inherits transformation optics (TO) [1, 2] to offer a new strategy of molding electromagnetic waves using isotropic materials [3–10]. However, this direct method to invert the wave equation mainly replies on the hard-core techniques of solving partial differential equations (PDE) from separation of amplitude and phase [4, 6]. Moreover, the solved material parameters were presumed passive without source or sink, which are violated in the non-Hermitian (NH) reality [11, 12] with both loss and gain to reshape the waves otherwise. We are then tempted to encode the non-Hermiticity into the inverse design for wave optics.

Surprisingly, all it takes is an isotropic material profile of *complex* value embracing loss and gain in a nutshell. Inspired by the synergy between NH photonics and TO [13], we extend the material parameters to a complex function of space to include loss and gain, and then develop a curved-space analogue picture in the spirit of TO. The imaginary part for the material profile immediately clarifies the inverting method, as we will derive below with ease in (3). Here the imaginary part of material profile (also for permittivity) is to encapsulate spatial gain and loss within access to metamaterial engineering [14]. We envision further that this theory shall blaze new trails of controlling wave flows in the NH landscape, which are ready to be implemented on the silicon photonic platform along with laser technology.

II. THEORY

We start from the Helmholtz equation in two dimensions for simplicity, which describes the wave transport and scattering behavior of a linearly polarized electric field with wavelength $\lambda_0 = 2\pi/k_0$ in an isotropic material. And the incidence wave $E_{\text{in}}(x, y)$ in air satisfies $\nabla^2 E_{\text{in}} + k_0^2 E_{\text{in}} = 0$. For a total wave $E(x, y)$ passing through a medium with refractive index $n(x, y)$, the Helmholtz equation goes as follows

$$\nabla^2 E + k_0^2 n^2(x, y) E = 0, \quad (1)$$

where the total wave solution is added by the incidence wave $E_{\text{in}}(x, y)$ and the scattering part $E_{\text{sc}}(x, y)$,

$$E(x, y) = E_{\text{in}}(x, y) + E_{\text{sc}}(x, y), \quad (2)$$

where E_{sc} is the scattered field scattered from the interaction between the wave and the medium. Using (2), the material parameter of the medium $n(x, y)$ is obtained by inverting (1).

$$n(x, y) = \sqrt{\frac{k_0^2 E_{\text{in}} - \nabla^2 E_{\text{sc}}}{k_0^2 E}}. \quad (3)$$

Therefore (3) gives the design medium as the central result in this work [15]. The wave solutions in (2) are complex functions of frequency and space in polar form [4], thus naturally enabling the NH medium where the imaginary index stands for sink and source in the media. Our inverting method shall provide sufficient room to manipulate waves, which we shall illustrate via three types of examples in Sec. III: controlling the amplitude, the phase, and the propagating direction.

III. EXAMPLES

A. Amplitude Controlling

As a simplest example – modulating the amplitude of a plane wave, we imagine a plane wave with phase

* Corresponding author: yangjie@hubu.edu.cn

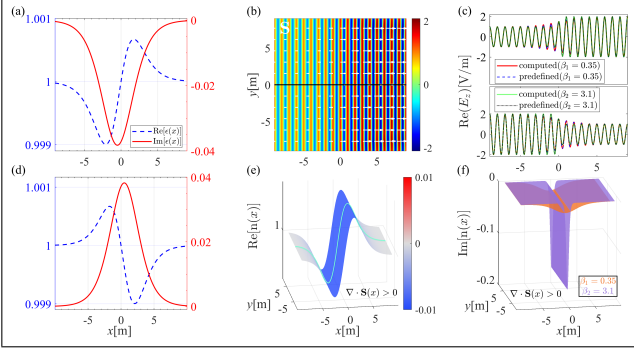


FIG. 1. Amplitude modulation of a plane wave by two NH media: (a) gain medium vs. (d) loss medium in permittivity profiles; (b) electric field distribution in the gain medium with white arrows indicating the Poynting vector; (c) matched fields of computation and predefinition for both media, which also include comparison of varied β values to tune the variance; (e) schematic of wave propagation in the gain medium (a); (f) imaginary parts of refractive index under different β values for the gain medium (a), which aligns with a positive divergence of Poynting vector $\nabla \cdot \mathbf{S} > 0$ representing a wave source negative in $\Im[n(x,y)]$.

$\exp(ik_0x)$ propagating through the design medium along $+x$ direction $\exp(-i\omega t)$ as convection [13]), and its amplitude is requested to vary smoothly from A_1 to A_2 for both ports of input and output while preserving its phase all along. Then the modulated plane wave shall carry a position-dependent amplitude $A(x)$:

$$A(x) = A_1 + (A_2 - A_1)f(x), \quad (4)$$

where $f(x) = [1 + \tanh(\beta x)]/2$ transits smoothly from A_1 to A_2 . Then the wave solution in the medium is $E(x) = A(x)\exp(ik_0x)$. Thus, from (2) the hence-scattered part should be

$$E_{\text{sc}}(x) = f(x)(A - A_1)\exp(ik_0x). \quad (5)$$

Substituting $E_{\text{in}} = A_1\exp(ik_0x)$ and (5) into (3) gives

$$n(x) = \sqrt{1 - \frac{(A - A_1)f''(x)}{k_0^2[A_1 + f(x)(A - A_1)]} - i\frac{2(A - A_1)f'(x)}{k_0[A_1 + f(x)(A - A_1)]}}. \quad (6)$$

In this manner, the incidence wave interacts within medium $n(x)$ progressively in (6) and then results in another planar wave with amplitude A_2 .

For a gain medium to increase $A_1 = 1\text{V/m}$ to $A_2 = 2\text{V/m}$ an index profile in Fig. 1(a) is obtained from (6). And the numeric field $E(x)$ for the wave walking through our design medium in Fig. 1 (b) verifies our theory in (6) in the upper part of Fig. 1 (c) for $\Re[E_z]|y=0$. One may reverse the propagation direction to achieve a shrunk amplitude shifting the other way round ($A_1 = 2\text{V/m}$, $A_2 = 1\text{V/m}$) as presented in the lower of Fig. 1(c), via a loss medium in Fig. 1(d) whose real permittivity is reverse in space and whose imaginary permittivity is complex conjugate to the gain medium in Fig. 1(a).

Curved surface analogue: the non-Hermitian (NH) medium can be understood as a curved, coloured surface in a nutshell as shown in Fig. 1(e), where its height depending on spatial dimensions represents the real part of the refractive index $\Re[n(x,y)]$ [16], and the colour gradient indicates its imaginary part $\Im[n(x,y)]$. Then the wave-flowing picture in Fig. 1(b) corresponds to the light trajectory in aquamarine on the curved surface in Fig. 1(e), under the combined dictation of the complex refractive index $n(x,y)$. Note that the complex permittivity profiles in Figs. 1(a) and (d) both strikingly resemble the linear susceptibility by Lorentz dispersion of the atom [17]. The trajectory follows the geodics on the surface governed by the real part, and the wave amplitude is controlled by the negative imaginary for energy gain during propagation in this case. Another tuning parameter for transition is parameter β in $f(x)$, which directly controls the degree of amplitude variation for amplitude. In Fig. 1(c), varying β from $\beta = 0.35$ to 3.1 sharpens the amplitude variation from A_1 to A_2 . And a close-up of imaginary refractive index in Fig. 1(f) reveals such a distinction, i.e., a steeper surface of the imaginary refractive index in purple points to a more rapid amplification, while the gentler slope in orange indicates a slower one. For the gain/loss degree of freedom, a positive divergence of Poynting vector $\nabla \cdot \mathbf{S} > 0$ in Fig. 1(f), represents a wave source with negative index $\Im[n(x,y)] < 0$, and a negative divergence $\nabla \cdot \mathbf{S} < 0$ indicates a sink instead with positive imaginary index $\Im[n(x,y)] > 0$.

B. Phase conversion

Other than amplitude controlling in Subsec. 3III A, we now in Subsec. 3III B turn to manipulate the wave phase via two cases. For an incident planar wave, we are equipped to design its phase $S(x,y)$ to smoothly shift away from planar to otherwise. So for a total wave $E = \exp(iS)$ [18], and from (3) we have the designed medium

$$n = k_0^{-1} \sqrt{(S'_x)^2 + (S'_y)^2 - i(S''_{xx} + S''_{yy})}. \quad (7)$$

We shall give three cases to illustrate the principle in (7). The first medium modulate one wave number to another, and the second converts the linear phase to a quadratic front in a continuous manner during propagation through. And the third works to convert it from planar to cylindrical. In all cases in Subsec. 3III B, one designs the one-dimensional phase $S(x)$ to follow

$$S(x) = S_1 + (S_2 - S_1)f(x), \quad (8)$$

similar to (4) where only S_2 is exemplified in each case.

Modulated planar phase: to design a medium that modifies the phase of an incident plane wave from $S_1 = k_0x$ to $S_2 = k_1x$, one yields the material profile illustrated in Fig. 2(a) by substituting (8) into (7), and the wave field form through this medium is shown in

Fig. 2(b). The simulated wave field in Fig. 2(b) validates that the medium manages to decreases the wave number from k_0 to k_1 in phase. The curved surface analogue for the conversion medium is also illustrated in Fig. 2(c), where the ray propagates along the aquamarine line and the imaginary index is mainly lossy as a sink on the surface.

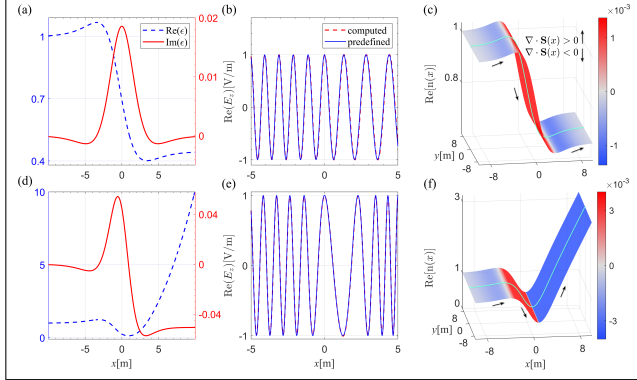


FIG. 2. Phase conversion from k_0x to k_1x (with $k_1 = 2k_0/3$) via a NH medium: (a) distribution of the permittivity; (b) electric field along x axis for comparison between computed and predefined fields; (c) curved surface analogue with coloured imaginary. Phase conversion from k_0x to $k_0^2x^2$ similarly: (d) - (f). In both panels (c) and (f), positive divergence of Poynting vector $\nabla \cdot \mathbf{S} > 0$ represents a wave source with negative index $\text{Im}n(x, y) < 0$, and a negative divergence $\nabla \cdot \mathbf{S} < 0$ does a wave sink with positive imaginary index $\text{Im}n(x, y) > 0$.

Quadratic phase: one may alter the phase from linear k_0x to quadratic $k_0^2x^2$, i.e. using $S_2 = k_0^2x^2$ to design a material shown in Fig. 2(d). The wave forms in Fig. 2(e) then confirms such a conversion into quadratic phase. The surface picture in Fig. 2(f) reveals that a sink at the conversion region and a source are collaborated to achieve just the quadratic phase in the designed region.

2D phase conversion-from plan wave to cylindrical wave: we now convert the phase further in two-dimensional (2D), by designing to transform the planar phase into cylindrical as if through a lens [19, 20]. The resultant phase in (8) shall become 2D: $S(x, y)$, by pre-defining the exit phase S_2 as if emitted from the virtual source $(-b, 0)$:

$$S_2(x, y) = k_0 \sqrt{(x + b)^2 + y^2}. \quad (9)$$

By substituting (9) into (7) and (8), the real and the imaginary parts of the index profile are shown respectively in Figs. 3(a) and (b). As the plane wave walks through the designed medium, the electric field converts its phase from planar to cylindrical smoothly, as shown in Figs. 3(c) and (d) [21]. However, the calculated fields in Fig. 3(b) reveal slight discrepancy under (near $x = -3$) and over (near $x = 1$) prediction. This deviation is primarily attributed to imperfect absorption of boundary-reflected waves by PML(cf. footnote 2) despite accurate wavefront modulation from plane to cylindrical. We

note that a passive medium [4, 6] cannot achieve similar waves which results in mismatched amplitude [data not shown]. This highlights the design power from the synergy by distributed source and sink (imaginary permittivity) in Figs. 3(b) and (e). The spatial distribution of the refractive index is presented as a curved surface in Fig. 3(e) with aquamarine light rays. And Figs. 3(f) depicts the contours for the real ($\Re[n(x, y)]$, red line) and the imaginary indices ($\Im[n(x, y)]$, blue line) which are non-orthogonal and henceforth non-conformal to each other [13]. Notably, the imaginary part of the refractive index exhibits a gain region near the source point [cf. Figs. 3(b) and (e)], in order to induce the cylindrical wave front from there. And the loss region near $0 < x < 5$ works to damp down the wave field just to maintain the unity amplitude predefined throughout Subsec. 3III B.

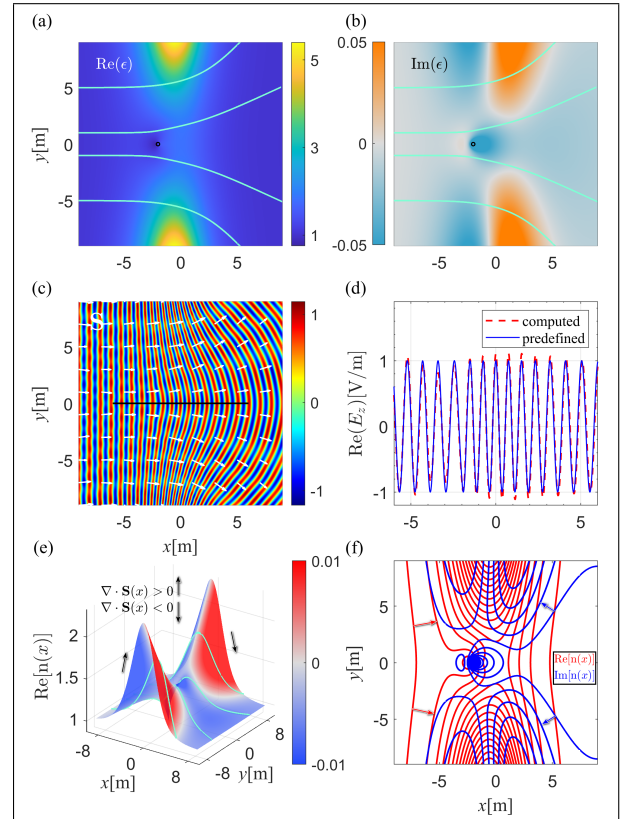


FIG. 3. Conversion of plane-wave phase to cylindrical-wave phase in a NH medium. (a, b) Distribution of the complex permittivity and note the virtual point $(-b, 0)$ marked by circles; (c) electric field distribution; (d) comparison between predefined and simulated electric fields along the black line in (c); (e) schematic of wave propagation through the designed medium; (f) contour plots showing the real and imaginary parts of the refractive index, both with an arrow indicating the increasing directions. Parameter: $b = 2$.

IV. AN ISOLATOR TO SHUNT THE WAVE DIRECTION

With an envelope-back derivation, one finds that for a complex conjugate medium, wave fronts can be swapped to achieve reciprocity. That being said, the very same medium will mold the inverted wave front from the other side different than the original one, and is henceforth *nonreciprocal*. So we design an isolator to shunt the wave vector to a specific direction, which should work only unidirectional, i.e., in one direction to shape the wave as predicted but not in the reverse one. Fortunately this scenario still boils down to the phase converter in Subsec. 3III B. Therefore, for a predefined wave phase of an obliquely exit vector related to the exit angle θ ,

$$\mathbf{k}_2 = k_0(\hat{x} \cos \theta + \hat{y} \sin \theta). \quad (10)$$

Thus one may design a NH medium under the periodic boundary condition along vertical y axis, so as to mold such a shunt phase. However, the predicted shunting turns out to work only for discrete exit angle θ ,

$$\theta = \arcsin \frac{2\pi n}{k_0 \Lambda}, \quad (11)$$

which derives from the condition for the transverse wave vector $k_y = 2n\pi/\Lambda$ and Λ is the length in vertical direction along one vertical period with n an integer.

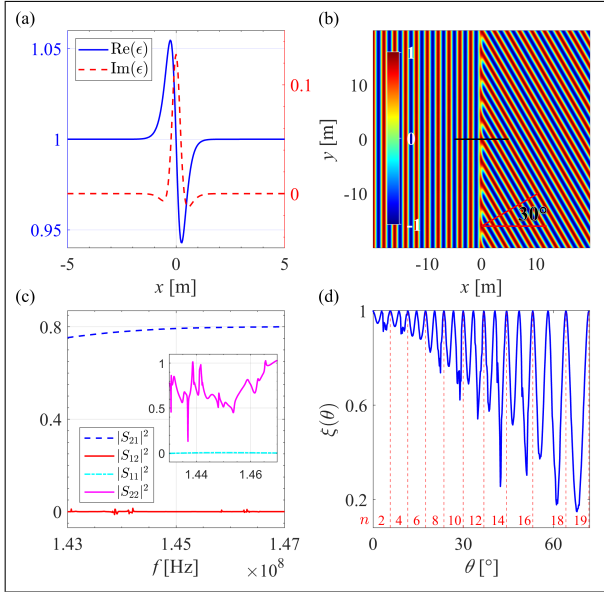


FIG. 4. Isolator medium: (a) material parameter uniform in vertical direction; (b) electric field distribution when the incident plane wave is deflected from $\theta|n=0$ to exit at $\theta|n=10$; (c) four power ratios of reflection and transmission (inset) in scattering matrix \mathbf{S} ; (d) relative accuracy of the calculated field E_c compared to the predefined E_p at different exit angles, which is defined as $\xi(\theta) = 1 - [\iint |E_c - E_p|^2 dS / \iint |E_p|^2 dS]^{1/2}$.

An example of the angle $\theta|n=10$ is presented in Fig. 4. For a complex refractive index in Fig. 4(a) within a

rather narrow region, the incident planar wave is converted towards the predicted direction $\theta(n=10)$, as shown in Fig. 4(b). The pronounced optical isolation behaviour [22] is confirmed by its high contrast transmission for S_{21} and S_{12} [23] for a frequency range of 4MHz depicted in Fig. 4(c), which demonstrates the asymmetric feature – a high forward transmission reaching 0.8 (due to loss region near $x=0$) along with severe suppression of backward propagation [24]. To quantitatively access the shunting effects for different exit angles, the relative accuracy $\xi(\theta)$ of the calculated field from prediction peaks sharply at unity as shown in Fig. 4(d) [blue curves], aligning with discrete angles in (11) [red dashed].

V. CONCLUSION

In a nutshell, we extend to the NH regime our previous inverting method to design isotropic profiles from known waves, encapsulating the source and sink in a coherent curved-space picture. By using three types of examples we find out that this method not only avoids the index range below unity [13], but also facilitates precise manipulation of wave phases beyond convectional Hermitian paradigms [6, 25]. This NH design tool may lead to further disruptive manipulation for light such as coherent perfect absorption [26], invisibility [5] and lasing [27], and contribute to the design arsenal of inverse problem in nanophotonics [28, 29].

ACKNOWLEDGMENTS

Funding National Natural Science Foundation of China (Grant Nos. 62571212, U25D8012), Science and Technology Department of Hubei Province (2024AFA038, 2022CFB553, 2022CFA012), Program of Outstanding Young and Middle-aged Scientific and Technological Innovation Team of Colleges and Universities in Hubei Province (T2020001), the Wuhan City Key R&D program (2025050602030069), and 2023 supplemental grant for 1A0702E004: Modern Optics.

Acknowledgment Y. L. thanks Mao Zhu, Sun Zizhuang, Jin Luling from Hubei University, and Han Song from Zhejiang University for their helpful discussions, and is especially grateful for the original idea by Simon Horsley from University of Exeter.

Disclosures The authors declare no conflicts of interest.

Data availability Data underlying the results presented in this paper are not publicly available at this time but may be obtained from the authors upon reasonable request.

-
- [1] J. B. Pendry, D. Schurig, and D. R. Smith, *Science* **312**, 1780 (2006), <https://www.science.org/doi/pdf/10.1126/science.1125907>.
- [2] U. Leonhardt and T. Philbin, *Geometry and light : the science of invisibility*, Dover books on physics (Dover Publications, Inc., Mineola, N.Y., 2010) p. 278.
- [3] T. G. Philbin, *Journal of Modern Optics* **61**, 552 (2014).
- [4] B. Vial, Y. Liu, S. A. R. Horsley, T. G. Philbin, and Y. Hao, *Phys. Rev. B* **94**, 245119 (2016).
- [5] T. G. Philbin, *Journal of Optics* **18**, 01LT01 (2016).
- [6] Y. Liu, B. Vial, S. A. R. Horsley, T. G. Philbin, and Y. Hao, *New Journal of Physics* **19**, 073010 (2017).
- [7] C. King, S. Horsley, and T. Philbin, *Phys. Rev. A* **97**, 053818 (2018).
- [8] S. Yu, X. Piao, and N. Park, *Phys. Rev. Lett.* **120**, 193902 (2018).
- [9] K. G. Makris, I. Krešić, A. Brandstötter, and S. Rotter, *Optica* **7**, 619 (2020).
- [10] I. Krešić, K. G. Makris, and S. Rotter, *Laser & Photonics Reviews* **15**, 2100115 (2021), <https://onlinelibrary.wiley.com/doi/pdf/10.1002/lpor.202100115>.
- [11] R. El-Ganainy, K. G. Makris, M. Khajavikhan, Z. H. Musslimani, S. Rotter, and D. N. Christodoulides, *Nature Physics* **14**, 11 (2018).
- [12] S. A. R. Horsley, M. Artoni, and G. C. La Rocca, *Nature Photonics* **9**, 436 (2015).
- [13] I. Krešić, K. G. Makris, U. Leonhardt, and S. Rotter, *Phys. Rev. Lett.* **128**, 183901 (2022).
- [14] D. Ye, C. Cao, T. Zhou, J. Huangfu, G. Zheng, and L. Ran, *Nat Commun* **8**, 51 (2017).
- [15] Here we take the root with the positive real part throughout this paper although the other could well work as the negative-index medium.
- [16] Y. Liu and L. K. Ang, *Scientific Reports* **3**, 3065 (2013).
- [17] R. W. Boyd, *Nonlinear Optics*, 4th ed. (Beijing World Publishing Corporation, Beijing, 2025).
- [18] N. Ossi, S. Chandramouli, Z. H. Musslimani, and K. G. Makris, *Optics Letters* **47**, 1001 (2022).
- [19] B. Lu, Z. Jiang, and D. H. Werner, *IEEE Antennas and Wireless Propagation Letters* **13**, 1779 (2014).
- [20] D. Isakov, C. J. Stevens, F. Castles, and P. S. Grant, *Advanced Materials Technologies* **1**, 1600072 (2016).
- [21] A Perfectly Matched Layer (PML) is applied at the boundaries of the computational domain to effectively absorb outgoing waves and eliminate spurious reflections, thereby enabling accurate numerical calculation of plane wave propagation in the designed medium.
- [22] D. Jalas, A. Petrov, M. Eich, W. Freude, S. Fan, Z. Yu, R. Baets, M. Popović, A. Melloni, J. D. Joannopoulos, M. Vanwolleghem, C. R. Doerr, and H. Renner, *Nature Photonics* **7**, 579 (2013).
- [23] C. Poole and I. Darwazeh, in *Microwave Active Circuit Analysis and Design*, edited by C. Poole and I. Darwazeh (Academic Press, Oxford, 2016) pp. 167–204.
- [24] C. Garcia-Meca and C. Barcelo, *Physical Review Applied* **5** (2016), 10.1103/PhysRevApplied.5.064008.
- [25] A. Yan, Y. Liu, and W. Wang, *Journal of Advanced Dielectrics* , 1950019 (2019).
- [26] Y. D. Chong, L. Ge, H. Cao, and A. D. Stone, *Phys. Rev. Lett.* **105**, 053901 (2010).
- [27] P. Bai, J. Luo, H. Chu, W. Lu, and Y. Lai, *Optics Letters* **45**, 6635 (2020).
- [28] A. Y. Piggott, J. Lu, K. G. Lagoudakis, T. M. Petykiewicz, J. and Babinec, and J. Vuckovic, *Nat. Photon.* **9**, 374 (2015).
- [29] S. Molesky, Z. Lin, A. Y. Piggott, W. Jin, J. Vuckovic, and A. W. Rodriguez, *Nature Photonics* **12**, 659 (2018).